

An Integrated Two-dimensional Geophysical Investigation of an Earth Dam in Zaria Area, Nigeria.

Chii E. Chii

Department of Physics, Adamawa State University, Mubi, Nigeria.

chiemma@gmail.com

Abstract: In order to investigate the subsurface seepage conditions of the Ahmadu Bello University farm dam in Zaria, we carried out a two-dimensional seismic refraction and electrical resistivity survey along a profile spanning the axis of the embankment. The ABEM Terrameter SAS 4000 supplemented with the ABEM Lund, multi-electrode, imaging system was used to obtain the electrical resistivity data and the data processed using the RES2DINV software. Also, seismic waves generated from multiple shots along the survey profile were recorded at closely spaced receivers installed along the profile using a 24 channel ABEM Terraloc Mk 6 seismograph. The seismic data were analyzed using REFLEXW version 3.0 interpretation software. Results show that the anthropogenic, lateritic clay material of the embankment has thickness ranging from 4 m to 12 m with p-wave velocity ranging from 372 m/s to 937 m/s and electrical resistivity ranging from 40 ohm-m to 85 ohm-m. The resistivity tomogram shows evidence of inhomogeneity in the near-surface embankment materials; this is an indication of differential saturation interpreted to be associated with differential compaction and or internal erosion. The seismic tomogram shows that the underlying gneissic bedrock (1878 to 3383m/s) is capped by a relatively lower seismic velocity zone in the range of 937 to 1690 m/s. This zone, with an average thickness of 4m, falls within the low resistivity range of 40 to 85 ohm-m. It is interpreted to represent a highly weathered and saturated portion of the bedrock and the suspected seepage pathway for water from the impounding reservoir. [Nature and Science 2010;8(10):358-368]. (ISSN: 1545-0740).

Key words: geophysical investigation; subsurface seepage conditions; earth dam; Nigeria

1 Introduction

Earth dams need periodic inspection and monitoring against the development of anomalous seepage paths either through the embankment, foundation or the abutment materials. Anomalous seepage is one of the major reasons for embankment dam failures and geophysical methods have the ability to detect anomalous seepage paths at an early stage before the safety and integrity of the dam are at risk (e.g. Bogoslovsky and Ogilvy, 1970; Butler *et al.*, 1989; Abuzeid, 1994; Sirls, 1997; Aal Gamal *et al.*, 2004; Lim *et al.*, 2004; Song *et al.*, 2005).

The Ahmadu Bello University (A.B.U.) farm dam is a homogeneous earth dam constructed in 1966 and is for the first time, subjected to an intensive geophysical investigation involving electrical resistivity and seismic refraction tomography. The aim is to identify weak zones which are responsible for seepage of water from the reservoir and to provide geophysical information required for the repair and maintenance of the dam.

Physical Environment, Geology and Hydrogeology of the Study Area

Zaria is situated within the highly degraded *Guinea Savanna* which has been mostly converted to farm land. It has a typical Savannah climate of distinct wet and dry seasons, with a moderate rainfall of about 1,047 mm/a. The rainy season usually starts in May and ends in October and the dry season last from late October to April (Walter, 1977).

The impounding reservoir together with its Watershed is underlain by biotite gneiss belonging to the Precambrian basement complex of northern Nigeria (Fig.1). It is therefore a metamorphic terrain bounded in the west by quartz-mica schist and in the east by biotite granite believed to have intruded the basement gneiss during the Pan African Orogeny according to McCurry (1970). The greater part of the area is covered by thick regolith mainly derived from *in-situ* weathering of the basement rocks. Some areas on the watershed are capped by lateritic material.

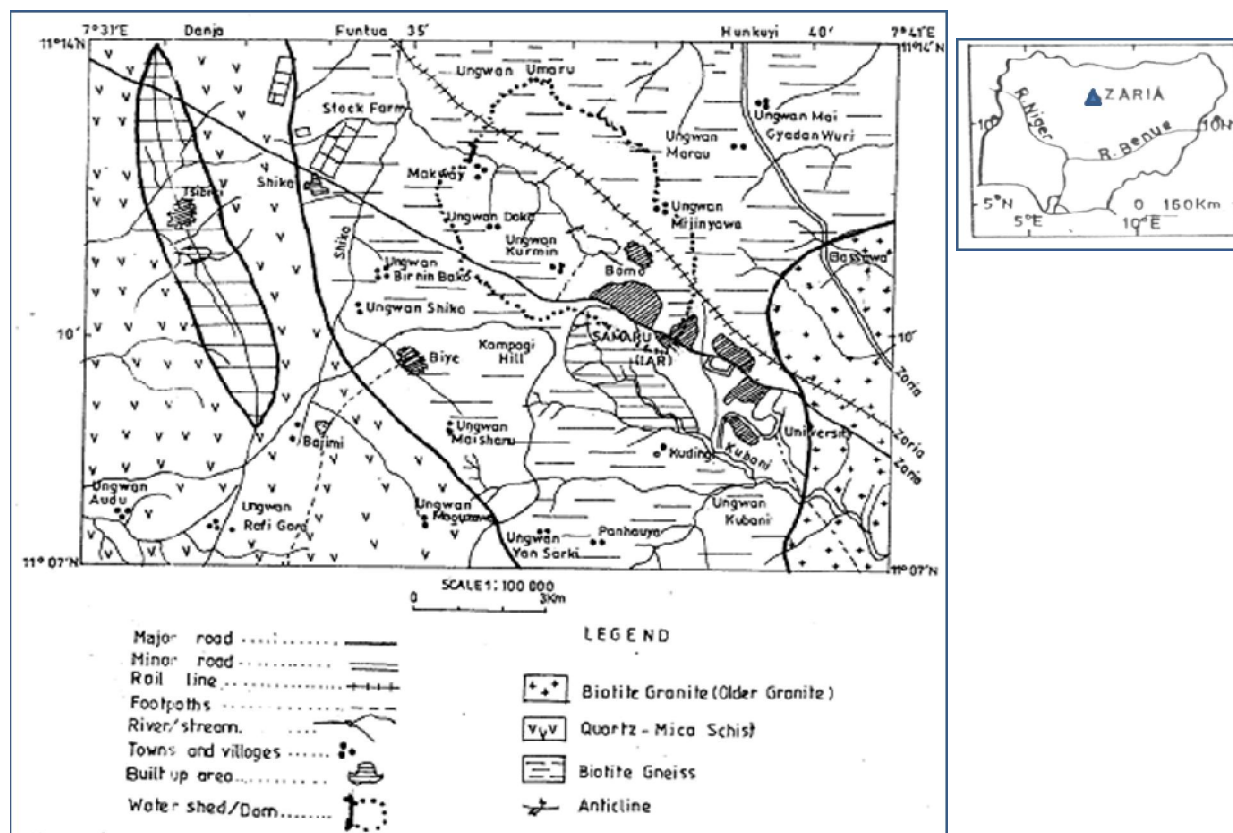


Figure 1. Geological map of the study area (McCurry, 1970)

2 DATA ACQUISITION:

2.1 Electrical Resistivity Data

Resistivity determinations are usually made by injecting a specified amount of electric current into the ground through a pair of current electrodes and then, with the aid of a pair of potential electrodes, measure the potential difference between any two points at the surface caused by the flow of the electric current in the subsurface. From the measured current (I) and the voltage (V) values, the ensuing resistivity is determined. A systematic arrangement of the two pairs of electrodes leading to Wenner or Schlumberger array is usually adopted depending on the nature of the resistivity survey to be carried out.

The ABEM Lund Imaging system comprising Terrameter SAS 4000 supplemented with an automated multi-electrode system (the electrode selector) was used in collecting the 2D electrical resistivity data. The Wenner32SX protocol dedicated

for Wenner- CVES roll-along measurement with 2 cables was employed because of its high signal – to – noise ratio. The 300 m long profile was taken on the crest of the dam spanning its entire axis (figure 2) at a unit electrode spacing of 5 m. Figure 3 shows the sequence of measurement to build a pseudo section from 20 electrode positions thus with raw data comprising of the determined apparent resistivity registered at each dotted point in 6 depth levels (Loke, 2001). The system used in this work, however, uses 24 electrode positions.

2.2 Seismic Refraction Data

A high resolution seismic refraction data set was acquired on the same resistivity profile line (figure 2) using a sledge hammer and plate as source with source locations spaced at 2.5 m intervals. Geophones with natural frequencies of 10HZ spaced at 2.5 m intervals were connected to a 24 channel Terraloc mk6 seismograph with source - receiver offset range of 0-15 m at both ends of the profile giving a profile length of 87.5m. Such a close range

was needed to enhance the signal-to-noise ratio over the unconsolidated region of the embankment materials. It should be noted that the signal provided by the hammer at its contact with the plate is highly attenuated over the soft ground thereby reducing the frequency content of the generated data.

The length of the profile line (300 m) was covered by effective roll-along achieved by shooting through the first 12 geophones of a receiver spread (i.e. one cable) and then moving the first cable to the end of the spread. Real-time noise monitoring along side data collection was done to make sure that the noise level was significantly reduced each time a set of data was collected, also five stacks were done per shot thereby further ensuring a high signal-to-noise ratio.

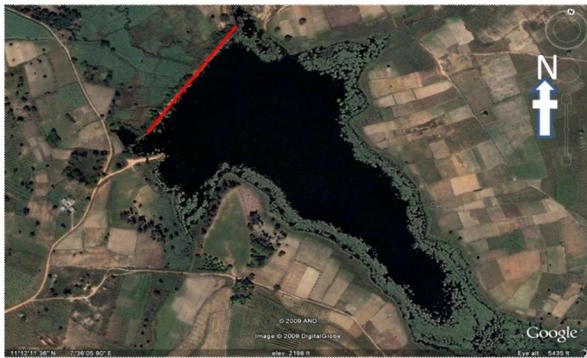


Figure 2. A satellite map of the reservoir of the A.B.U. farm dam with the profile line indicated on the embankment (Modified from Google Earth, 2009).

3 DATA ANALYSIS

3.1 Resistivity Data Analysis

The raw data were processed and analyzed using the computer program RES2DINV (Loke and Barker, 1996). The 2D model used by the program divides the subsurface into a number of rectangular blocks. The program then determines the resistivity of the rectangular blocks that produces an apparent resistivity pseudo section (calculated apparent resistivity) which agrees with the actual measurement.

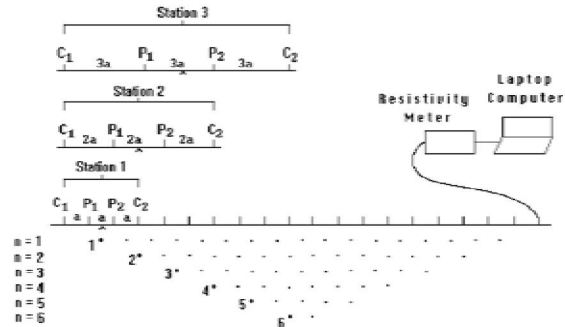


Figure 3. Sequence of measurements to produce a 2D electrical resistivity pseudosection using a computer controlled multi-electrode survey setup (Loke, 2001).

A finite-difference forward modeling subroutine was used to calculate the apparent resistivity values with a relatively dense mesh grid of 4 nodes per unit electrode spacing to increase the accuracy of the calculated apparent resistivity. The thickness of the first layer of blocks was set at 0.5 times the unit electrode spacing with the thickness of each subsequent deeper layer increased by 10%. The model discretization is such that the number of cells used was equal to the number of data points which is the best option for large data set of this nature (Loke, 2001). A non-linear least-squares optimization technique (deGroot-Hedlin and Constable, 1990; Loke and Barker, 1996) was used for the inversion routine. The optimization method basically tries to reduce the difference between the calculated and measured apparent resistivity values by iteratively adjusting the resistivity of the model blocks. A measure of this difference is given by the root-mean-squared (RMS) error. The model at the iteration after which the RMS error does not change significantly is usually considered the “best” model and in this work, this occurred at the 5th iteration.

One advantage of this method is that the damping factor and the flatness filters can be adjusted to suit different types of data. Since the data obtained in this work are less noisy, an initial damping factor of 0.1 was used and the minimum was fixed at 0.02 (one-fifth of the initial) to stabilize the inversion process). The inversion routine generally reduces the damping factor after each iteration and the smooth models obtained have the ability to suppress model structures not required by the data. The generated models therefore contain the minimum possible structures and is then likely that the true Earth is at least as rough as the models (deGroot-Hedlin and

Constable, 1990) thereby increasing the probability that identified anomalies are really existent.

3.2 Seismic Refraction Data Analysis

3.2.1 First-break Picking

The data analysis was carried out using the seismic refraction module of Reflexw version 3.0 software by Sandmeier (2003). It is a versatile

package that provides a wide range of processing and interpretation tools.

The raw data were first of all imported into the Reflexw environment (figure 4a shows a set of raw data traces for a shot point at 0m along the profile). Unwanted signals were removed by using band pass filtering and the filtered signal enhanced using a gain function. Picking of the first-arrival was manually done (figure 4b shows the enhanced signals with the first arrival picks (the red crosses)).

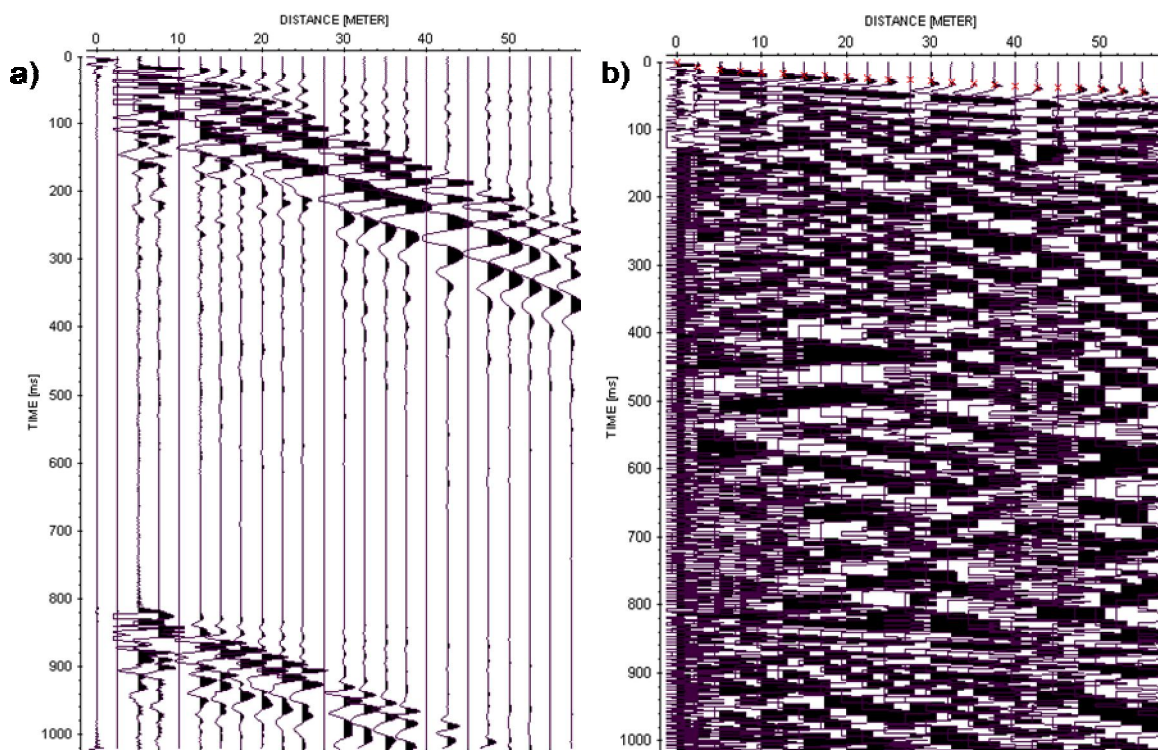


Figure 4. a) Raw data at a shot point 0m along the profile and (b) Enhanced data showing picked first-arrival

3.2.2 Traveltimes Processing

The traveltimes processing module of the software provides the possibility of putting together the picked travel-times from all the shots along the profile. Figure 5 shows all the picked travel-times curves along the profile. The picks are assigned to special layers (figure 6a and b). The forward and reverse distance-time plots for each of the six spreads constituting the profile (of which figure 6a is one of them) reveals a two layer case. The mean of the updip and downdip traveltimes for the first layer was assigned to the first layer within that segment of the profile and so was the traveltimes assigned to the remaining segments constituting the entire profile. The green lines in figure 6b show the segments of the traveltimes curves sampling the overburden while the blue lines are the segments sampling the basement.

Those traveltimes originating from several shots and belonging to a particular layer were combined to one complete forward and reverse traveltimes curves (Phantoming). Figure 6b shows one complete forward (red circles) and reverse (black circles) traveltimes curves automatically generated for the second layer. Analysis of the combined

forward and reverse traveltimes (insert at the top left hand corner of figure 6b) shows a difference between the maximum reverse and maximum forward traveltimes of 2.4151 ms (which is less than 5) indicating that the assignment of the traveltimes to layers is accurate. These combined traveltimes are the basis for a subsequent 2D wavefront inversion.

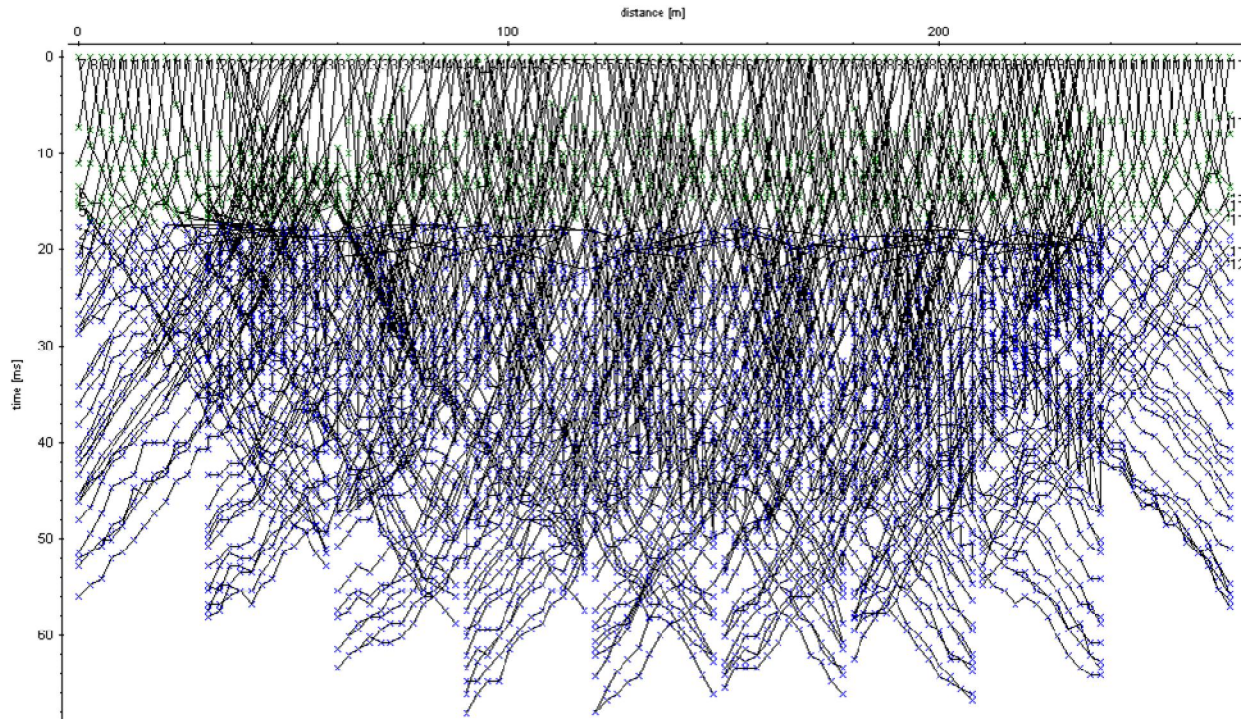


Figure 5. A combination of all the travel-times curves for all the shots along the profile

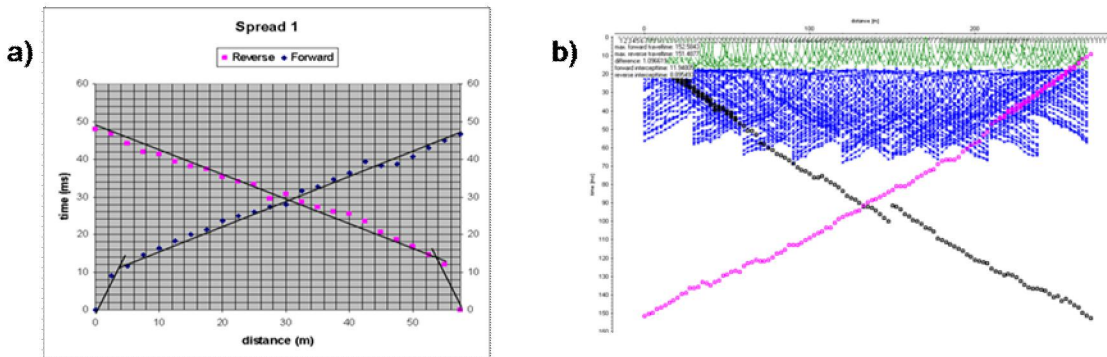


Figure 6 a. one of 6 forward and reverse travel time curves used for assignment of travel- time to layers ; Figure 6 b. Travelttime data put together and assigned to 2 different layers (the green represents the traveltimes segments corresponding to the first layer while the blue represents those for the second layer).

3.2.3 Wavefront Inversion

After phantomng, wavefront inversion was performed which enabled the migration of the combined forward and reverse traveltimes into depth using a Finite Difference approximation of the eikonal equation,

analogous to the forward ray tracing by Vidale (1988). We used a model grid with spatial increment of 0.5. This value was chosen to avoid any significant loss of overburden inhomogeneity and also as a compromise between a good resolution and cost in terms of computer time (computer time for the inversion increases by a factor of 4 if increment is decreased by a factor of 2).

The method is iterative, meaning that each layer must be inverted separately and that an overburden must exist. In inverting the first layer however, no overburden is necessary, but to invert the second layer, the overburden must be known. The first layer serves as overburden to the second layer and so on. When the option “wavefront-inversion” is activated for layer 1, the program automatically creates a new model consisting of the top layer boundary with layer points at the positions of the different traveltimes branches assigned to layer 1. The velocities at these positions are automatically determined by linear regression.

For the second layer, the complete forward and reverse wavefronts are continued downwards based on the given overburden model. The new refractor is automatically constructed at those points where the sum of the downward traveltimes is equal to the reciprocal traveltimes. The refractor velocity is determined from the mean of the slopes of the forward and reverse wavefronts at the new calculated refractor points (Sandmeier, 2003).

The end result of this process is interfaces of the layers and layer velocities which serve as initial model for subsequent tomographic inversion. Figure 7 shows the generated initial model, it is a two homogeneous layer case with overburden velocity of 430 m/s and the underlying layer of velocity of 1988 m/s.

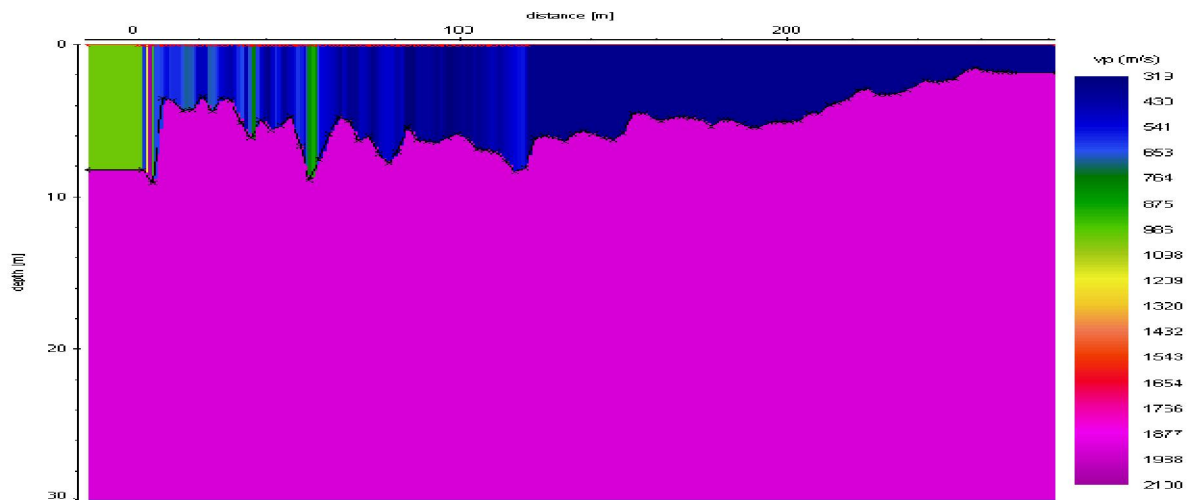


Figure 7. Initial model generated from wavefront inversion showing interface between the overburden and the underlying layer; it serves as input model for tomographic inversion.

3.2.4 Tomographic Inversion

To determine the true subsurface velocity structure from the recorded traveltimes, the package uses a tomographic algorithm that simulates the propagation of wavefronts through complex 2D heterogeneous media thereby computing the ray paths and travel times (figure 8) by finite-difference approximation of the eikonal equation (Vidale, 1988).

The simulation technique allows the automatic adaptation of the synthetic traveltimes data to real data based on a two-dimensional tomographic algorithm. The algorithm is based on, the Simultaneous Iterative Reconstruction Technique (SIRT). Starting from the initial model, the synthetic travel times are calculated using curved rays. These traveltimes are compared to the real (observed) ones and model changes (velocity distribution) are automatically derived from the travel time residuals. The procedure is repeated based on the changed model and stops when a distinct stopping criterion is fulfilled. In this case we used a stopping criterion of less than 2% model change and this was achieved after the 10th iteration. It takes into account the existence of different propagation waves like transmitted, diffracted or headwaves and therefore offers no practical limitation on the complexity of the medium.

This makes the method very suitable for near surface investigations of this nature since there is no need for approximation concerning the complexity of the model. The resulting velocity model is a raster file (tomogram) showing a range of velocities in colours, this result will be displayed in the following section.

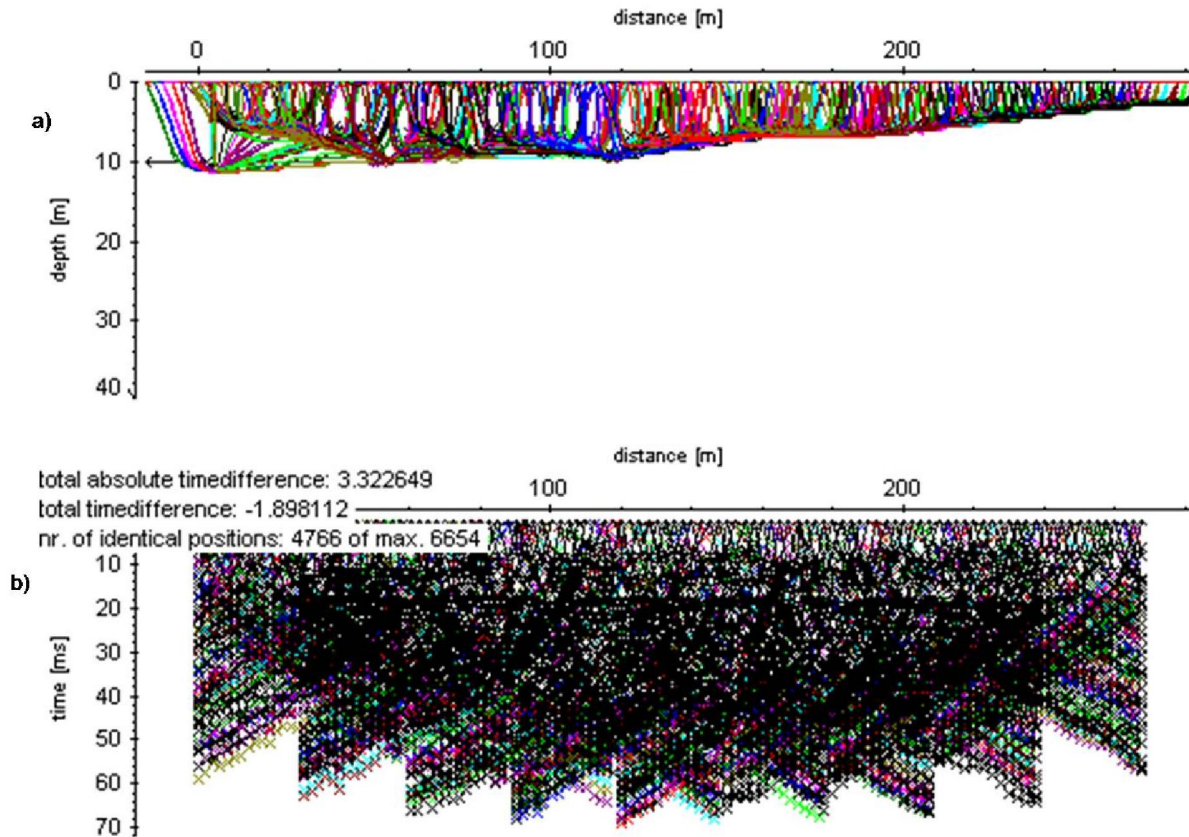


Figure 8a. Ray diagram and Figure 8b. Comparison of observed traveltimes (black) with the synthetic traveltimes (coloured) based on tomographic result (Inset is the traveltimes analysis showing total absolute time difference of 3.322649ms, total time difference of -1.898112 ms and number of identical positions of 4766).

4 RESULTS AND DISCUSSION

4.1 Resistivity Results

The complete set of geoelectrical images comprising the measured apparent resistivity pseudosection, the calculated apparent resistivity pseudosection and the inverse model resistivity section are shown in figure 9a, 9b and 9c respectively. The inverse model resistivity section of figure 9c, representing the true subsurface resistivity distribution was further interpreted using information from the geologic log of a borehole drilled within the study area (Table 1).

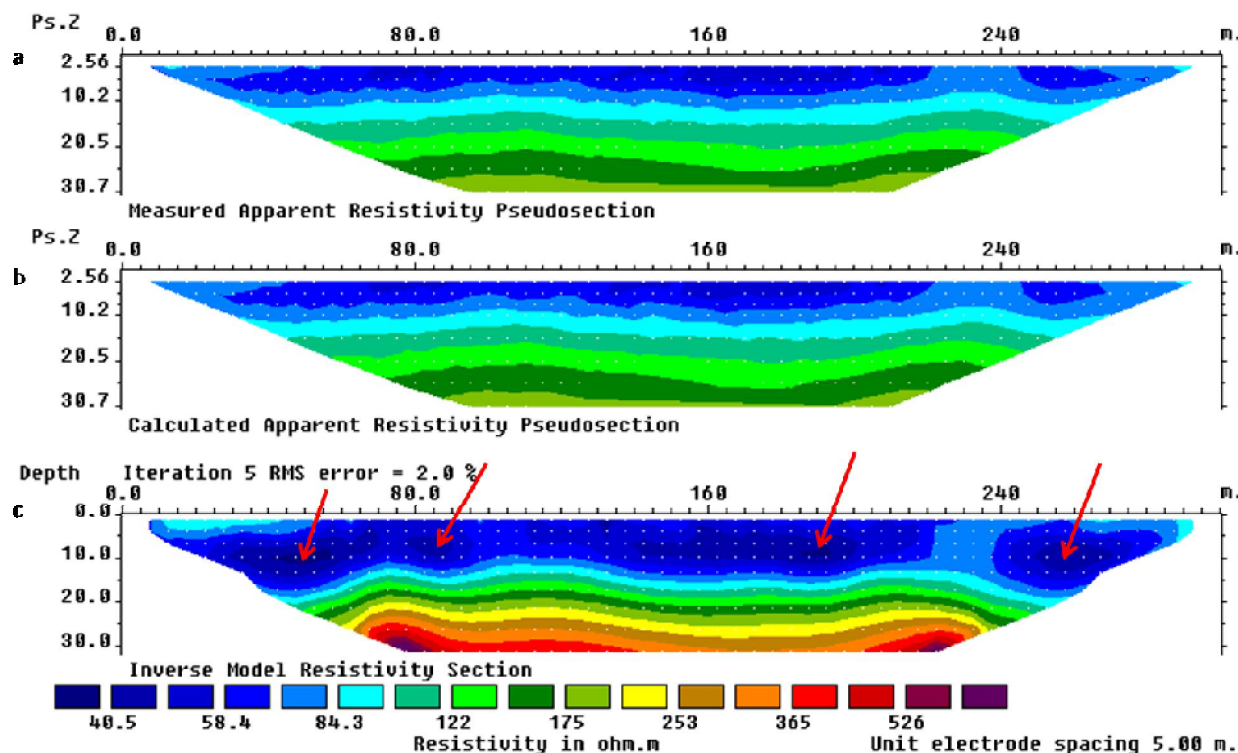


Figure 9. a) The observed and (b) the calculated apparent resistivity pseudo sections for the data set with (c) the subsurface model obtained from inversion. Arrows indicate zones of anomalously low resistivity.

Table 1: Lithology and aquifer of a borehole log drilled within the study area (NWRI, 2002)

Depth (m) of Occurrence		Thickness (m)	Lithology
FROM	TO		
0	15	15	Reddish brown laterite
15	21	6	Brownish sandy clay
21	42	21	Weathered basement
42	-	-	Fresh Crystalline Rock

Combining the information provided in Table 1 with the range of resistivity values obtained from the inverse model resistivity section (40-526 ohm-m), a lithological unit-based model classification is derived as shown in Table 2.

About eleven geoelectric segments are encountered in the inverse model resistivity section with each geoelectric segment represented by a distinct colour. The reliability of the inverse model resistivity section (Fig. 9c) is reflected in the degree of

agreement between the measured and calculated apparent resistivity pseudosections (Fig. 9a and 9b). This can be easily seen by visual inspection of the images of the two apparent resistivity pseudosections (Fig. 9a and b) and also from the low RMS error which is 2.0%.

Table 2. Model classification of lithology and resistivity from the data obtained

Rock types	Resistivity (m)
lateritic Clay	40-84
Highly weathered basement	84-175
Fairly weathered basement	175-1000
Fresh basement	>1000

The eleven geoelectric segments in the inverse model resistivity section constitute three distinct geologic layers based on the new classification (Table 2). The top layer with resistivity value ranging from 40 to 84 m and thickness of 10 m to 18 m is interpreted as a lateritic clay soil with

varied moisture content. The relatively low resistivity layer is underlain by a moderate resistivity layer (84 - 175 $\Omega\cdot\text{m}$) with average thickness of 10 m. This layer is interpreted as a highly weathered portion of the gneissic bedrock with the relatively moderate resistivity value due to saturation. A resistive layer with resistivity range from 175 to 526 $\Omega\cdot\text{m}$ is observed at a depth ranging from 23 to 25 m estimated from the crest of the dam. This zone represents a fairly weathered and less saturated portion of the bedrock. The fresh basement associated with resistivity value of 1000 $\Omega\cdot\text{m}$ and above was not encountered probably due to the limitation of the depth of investigation.

4.2 Seismic Refraction Results

Figure 10 is the final tomographic inversion result showing the subsurface p-wave velocity distribution of range 372-3383 m/s.

The ray diagram in figure 8a provides information on the reliability of the tomogram. The dense nature of ray paths down to a depth of about 12 m indicates a high resolution of the overburden. Ray coverage and therefore confidence in velocity estimates is reduced at depths greater than 12 m below the surface.

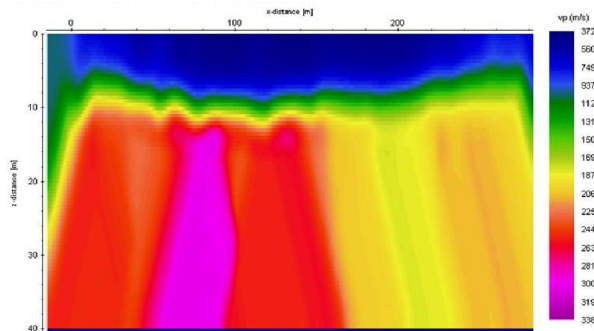


Figure 10. The seismic refraction tomogram showing the full range of p-wave velocities between 372 and 3383 m/s. (Vertically exaggerated).

Figure 8b shows how well the synthetic and observed traveltimes match. The traveltimes analysis shows between the synthetic and observed, total absolute time difference of 3.322649 ms, total time difference of -1.898112 ms and number of identical positions of 4766 out of 6654. This further emphasizes the reliability of the final tomographic result shown in figure 10.

Interpretation of this tomogram is also guided by the borehole log (Table 1) for the nearest borehole to the investigated area and standard P-wave velocities

(Table 3) of earth materials constituting the geology of the study area.

Table 3: Standard P-wave velocities of soils and rocks (Kearey and Brooks, 2002; Dobrin, 1976; Osemeikhian and Asokhia, 1994).

Material	P-wave velocity (m/s)
Air	300-330
Water	1400-1800
Alluvium sand (dry)	300-1000
Sand (water-saturated)	1200-2000
clay	1100-2500
Granite and gneiss	2000-6200

As expected, the near surface homogeneous embankment materials are represented by uniformly low velocities less than 937 m/s. This low velocity is associated with the unconsolidated nature of the anthropogenic lateritic clay construction materials of the embankment. There is noticeable thickening of this surface low velocity layer from the flanks (thickness of about 4 m) towards the centre of the spread (thickness of about 8 m). This represents the extent of excavation of the overburden along the river valley and final refill using the lateritic clay material. The boundary between this surface layer and the underlying undisturbed layer is concave which is a characteristic outline of a typical profile across a river valley. This is underlain by a moderate velocity zone of velocity ranging from about 937 to 1690 m/s representing a highly weathered and saturated portion of the gneissic bedrock with an average thickness of about 4 m. Beneath this weak layer, is the fairly weathered bedrock with velocities above 1690 m/s.

4.3 Combination of the Results of the Electrical Resistivity and the Seismic Refraction Analysis

Three layers of relatively uniform velocity of ranges 372 - 937 m/s; 937 - 1690 m/s and 1690 - 3383 m/s are delineated on the seismic tomogram in figure 10. The first layer is interpreted to represent the overburden comprising anthropogenic, lateritic clay embankment material. This layer shows variable thickness of about 8m around the centre of the profile, beneath the 180m point along the profile, and narrows towards the extreme ends of the profile where it is about 4m thick. The second layer of fairly uniform thickness of 4 m and velocity range 937 - 1690 m/s represents a highly weathered and saturated portion of the underlying gneissic bedrock. These two layers have been combined in the resistivity tomogram

(figure 9c) as one with an average thickness of 13m and resistivity range of 40 – 84 m (Note that resistivity is not directly a function of density; it depends on : porosity, permeability, connectivity of the pores, the nature of electrolyte contained in the pores, *etc.*). This is probably due to the fact that the denser material of velocity range 937 – 1690 m/s constituting the highly weathered basement and underlying the less dense embankment material of velocity range 372 –937 m/s is so saturated that its resistivity is the same with the overlying less consolidated material. In other words, a 4 m thick portion of the underlying gneissic bedrock constituting the foundation of the overlying lateritic clay embankment material is highly weathered and saturated. This layer (*i.e.* the intermediate layer of velocity 937-1690 m/s on the seismic tomogram) represents an anomaly of interest because such a weak formation either harbours microchannels and or favours the development of microchannels serving as seepage pathway for water from the impounding reservoir by hydraulic pressure.

Also, within the first layer of resistivity range 40 – 85 m on the resistivity tomogram is evidence of heterogeneity with portions of anomalously low resistivity of less than 40 m. This is interpreted to represent zones of weakness within the embankment (represented with arrows on the resistivity tomogram in figure 9c). The two possible explanations on their origin are as follows:

- i) This is interpreted to be associated with differential compaction, during the dam construction, which led to formation of weak zones resulting in differential saturation as the reservoir became filled up with water.
- ii) These are probable areas of internal erosion where the fine materials of the embankment have been washed out and their place taken up by water.

In either case, these weak zones are identified as anomalies of interest in this work as they could serve as conduit for seepage of water from the impounding reservoir. These are not identifiable on the seismic tomogram because of the inherent averaging characteristics of the seismic method which have rendered it not capable of detecting and delineating discrete bodies of this nature.

CONCLUSION

The problems of the dam, as revealed by this study, are defects in the embankment and the

foundation. Weak zones have been identified in the embankment as portions of anomalously low resistivity of less than 40 m on the resistivity tomogram. These weak zones are interpreted to be associated with differential compaction during the dam construction and or internal erosion taking place within the embankment materials where fine particles are being washed out from the embankment thus making the remaining materials to be very porous and saturated by water. Such weak zones within the embankment are identified as possible seepage pathway for water from the impounding reservoir and as the most dangerous anomalies associated with the dam as they can lead to the collapse of the embankment especially if filtration velocity increases to a certain threshold level.

Also a 4 m thick portion of p-wave velocity of 937 – 1690 m/s and electrical resistivity of 40 – 84 m, capping the gneissic bedrock underlying the embankment materials is highly weathered and saturated. Such a weak formation could harbour microchannels or could favour the development of microchannels serving as seepage pathway of water from the Impounding reservoir by hydraulic pressure. These probably account for all-year-round marsh at the down stream portion of the dam and the inability of the reservoir to be filled to capacity except at the peak of the raining season.

Results of the two methods along this profile have actually emphasised the need for integrated methods of geophysical investigation of this nature more especially when the methods complement one another.

We are recommending injection grouting for the weak zones identified within the embankment and a cutoff wall spanning the entire axis of the dam for the defective foundation.

Acknowledgement

I wish to acknowledge the International Programme in the Physical Sciences (IPPS) Uppsala University, Sweden for providing the equipment used in this work and part of the funding. Professor I.B. Osazuwa of the department of physics, Ahmadu Bello University, Zaria, Nigeria is acknowledged for supervising the work.

REFERENCES

- [1] Bogoslovystky VA, Ogilvy AA. Application of Geophysical methods for studying the technical status of earth dams. *Geophysical Prospecting* 1970; 18: 758 - 73
- [2] Butler KD, Llopis LJ, Deaver MC. Comprehensive geophysical investigation of an existing dam foundation, the Leading Edge of exploration. August 1989; 10-18.
- [3] Abuzeid N. Investigation of channel seepage areas at the existing Kaffrein dam site (Jordan) using electrical-resistivity measurements. *Journal of Applied Geophysics* 1994; 32: 163-75
- [4] Sirles P, Seepage investigation using geophysical techniques at Coursier Lake Dam, B.C., Canada. Symposium of the Geophysical Application to Environmental and Engineering Problems (SAGGEP), Reno-Nevada 1997; 1: 321-31.
- [5] Aal Gamal ZA, Ahmed MI, Neil LA, Estella A, Atekwana A. Geophysical Investigation of Seepage from an Earth Fill Dam, Washington County, Mo 2004; Available at www.dot.state.fl.us
- [6] Lim HD, Kim KS, Kim JH, Kwon HS, Oh BH. Leakage detection of earth dam using geophysical methods. *Procs. International Commission on Large Dams (ICOLD), 72th Annual Meeting, Seoul, Korea, 16-22 May 2004*: 212-24
- [7] Song SH, Song YH, Kwon BD. Application of hydrogeological and geophysical methods to delineate leakage pathways in an earth fill dam. *Exploration Geophysics* 2005; 36: 92-96
- [8] Walter, M. W. (1977): The Length of the Rainy Season in Nigeria. *Agricultural Meteorology* 1997;18(1): 313-22.
- [9] McCurry P. The Geology of Degree Sheet 21 Zaria. Unpublished MSc. Theses, Ahmadu Bello University Zaria 1970:20-22
- [10] Loke MH. *Electrical Imaging Surveys for Environmental and Engineering Studies. A Practical Guide to 2-D and 3-D surveys* 2001:10-12
- [11] Google Earth. Digital Globe 2009
- [12] Loke MH, Barker RD. Rapid least-squares inversion of apparent resistivity pseudosections by a quasi-Newton method. *Geophysical Prospecting* 1996; 44: 131- 52.
- [13] deGroot-Hedlin C, Constable S. Occam's inversion to generate smooth, two-dimensional models from magnetotelluric data. *Geophysics* 1990; 55:1613- 24.
- [14] Sandmeier K.J. Windows™ 9x/NT/2000/XP-program for the processing of seismic, acoustic or electromagnetic reflection, refraction and transmission data, Manual for REFLEXW 2003;3:1-177. (available at www.sandmeier-geo.de).
- [15] Vidale J. Finite-difference calculation of travel time *Bulletin of the Seismological Society of America* 1988; 78(6) 2062-76
- [16] NWRI. Borehole completion report at ABUTH Hostel, Groundwater Research Department, National Water Resource Institute, Kaduna, Nigeria 2002:1-10.
- [17] Kearey P, Brooks M. *An Introduction to Geophysical Exploration*. Blackwell 2002:1-255.
- [18] Dobrin MB. *Introduction to Geophysical Prospecting*. McGraw-Hill. 1976:630 - 50.
- [19] Osemeikhain J E, Asokhia M B. *Applied Geophysics For Engineers and Geologist Samtos Services Ltd Lagos, Nigeria*.1994:1-122.